ADVANCED ELECTRONIC MATERIALS
www.advelectronicmat.de

Nonvolatile Photoelectric Memory Induced by Interfacial Charge at a Ferroelectric PZT-Gated Black Phosphorus Transistor

Liu Xie, Xin Chen, Zhuo Dong, Qiang Yu, Xinxin Zhao, Guoliang Yuan, Zhongming Zeng, Yaojin Wang, and Kai Zhang**

Ferroelectric-field-effect-transistor (FeFET) memory, characterized by its nonvolatile, nondestructive readout operation and low power consumption, has attracted tremendous attention in the development of next-generation random-access memory. However, the electrical reading processes in conventional FeFETs may attenuate the ferroelectric (FE) polarization and lead to readout crosstalk. A photoelectric-type FeFET memory with alternative readout through 2D black phosphorus (BP)/lead zirconate titanate (PZT) heterostructures is developed. Based on charge-mediated electric-field control, a unique polarization-dependent photoresponse is observed, resulting in both positive photoconductivity (PPC) and negative photoconductivity (NPC) in a single device element via FE gating. This enables a nonvolatile photoelectric memory working in a novel "electrical writing-optical reading" process mode. Furthermore, the device exhibits a reliable data retention (over 3.6×10^3 s) and fatigue (exceeding 500 cycles) performance with extremely low energy consumption (driving voltage <10 mV). The demonstrated BP/PZT heterostructure memory devices show a pathway to high-performance photoelectric storage devices as light-activated logic gates for on-chip optical communications.

Nonvolatile memory, dominated by flash memory, plays a critical role in the modern electronic information industries.[1–3] Conventional metal-oxide-semiconductor field effect transistor-based flash memory is suffering the pronounced leakage current and weak charge storage capability with the size reduction.[4–7] To this end, ferroelectric random access memory (FeRAM) becomes one of the growing number of alternative technologies, which shows great advantages referring to the faster write performance and much greater maximum read/write endurance.[8,9] Traditional FeRAM is in a single capacitance structure, composed of ferroelectric (FE) materials with spontaneous polarization and top/bottom electrodes. It achieves two stable nonvolatile states as "0" and "1" to implement information storage with the application of electric fields.[10–13] Despite the great promise it holds, the commercial prospect of FeRAM is hampered by virtue of low integration. In particular, the read operation of FeRAM is destructive and reprogramming is needed after each readout process, resulting in high power consumption and prolonged readout time.[13,14] While, the drawbacks of a single capacitor-type FeRAM can be ameliorative if the device structure replaced by field effect transistor (FET), which benefits from its nondestructive readout operation and excellent compatibility with the current complementary metal-oxide-semiconductor technology.[15–18] By this means, the FE materials, served as gate insulator, are combined with semiconductors to form a synergistic heterostructure system with novel functionalities.

Relative to conventional semiconductors, 2D ones, such as transition metal dichalcogenides (TMDs)[19] and black phosphorus (BP),[20,21] are more suitable to construct of synergistic heterostructure devices. On one hand, 2D materials enable versatile heterostructure integration with other 1D, 2D, and 3D counterparts through van de Waals coupling. More significantly, atomically thin characteristic of 2D materials is prone to high integration density and provides convenience for gating tunability. Lead zirconate titanate (PZT)-gated few-layer graphene have been previously reported to process an extremely high mobility of $\mu \sim 7 \times 10^4$ cm^2 V^{-1} s^{-1}.[22] It has been also reported that FE material as gating dielectric can tune the transport behavior and improve electrical performance of the 2D FETs.[23–26] Thereby, the combination of 2D semiconductors and FE materials has potential to provide an excellent platform

Dr. L. Xie, Dr. Z. Dong, Q. Yu, Dr. X. Zhao, Prof. Z. Zeng, Prof. K. Zhang
CAS Key Laboratory of Nano-Bio Interface & Key Laboratory of Nanodevices and Applications
i-Lab
Suzhou Institute of Nano-Tech and Nano-Bionics (SINANO)
Chinese Academy of Sciences
Ruoshui Road 398, Suzhou, Jiangsu 215123, P. R. China
E-mail: kzhang2015@sinano.ac.cn

Dr. L. Xie, Dr. Z. Dong, Dr. X. Zhao
School of Nano Technology and Nano Bionics
University of Science and Technology of China
Jinzhai Road 96, Hefei, Anhui 230026, P. R. China

X. Chen, Prof. G. Yuan, Prof. Y. Wang
School of Materials Science and Engineering
Nanjing University of Science and Technology
Xiaolingwei Street 200, Nanjing, Jiangsu 210094, P. R. China
E-mail: yjwang@njust.edu.cn

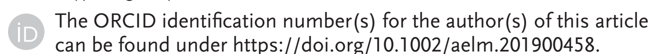
The ORCID identification number(s) for the author(s) of this article can be found under https://doi.org/10.1002/aelm.201900458.

DOI: 10.1002/aelm.201900458

© 2019 WILEY-VCH Verlag GmbH & Co. KGaA, Weinheim

for constructing nonvolatile memory and new functional devices. Doh et al. have fabricated graphene FETs with top-gate poly(vinylidenefluoride-trifluoroethylene) (P(VDF-TrFE)) organic film, which exhibit bi-stable resistance with a relatively long retention under the application of external bias.[27] The nonvolatile memory has been favored based on the graphene ferroelectric field effect transistor (FeFET); however, the on/off ratio of a graphene-based transistor is small due to its zero bandgap. In turn, 2D semiconductors, such as TMDs, BP have trigged great attraction as the channel of FeFET for nonvolatile memories.[18,28–31] Despite some progress, these organic FE gate–based devices still encounter obstacles including slow switching speed, high operation voltage, slow dipole dynamics, and low durability.[29,30,32] To address these challenges, Ko et al. has demonstrated superior nonvolatile memory performance with 2D TMDs FETs using PZT thin films as back gate.[14] The devices exhibit low operation voltages of 2.5 V, high on/off ratio of 10^4, and reliable data retention of 10 days.

It is noteworthy that above demonstrated 2D/FE FET-type nonvolatile memory devices are relying on the electrical manipulation and record. Depolarization field during the electric reading processes may not be eliminated and is the main reason for weakening the FE polarization, where the electrical reading processes relying on the current on/off ratio lead to the issue of readout crosstalk in virtue of ferroelectric polarization loss. Consequently, alternative stably nondestructive readout methods are in serious demand, and in particular the photoelectric memory has been proposed and attracted great attentions because the photoelectric storage devices with capability of light-activated logic gates, is compatible and of central importance for the development of on-chip optical communication technology. Based on ferroelectric polarization-dependent photovoltaic effect, a nondestructive photoelectric memory operating in the visible range has been demonstrated in a typical FE capacitor.[13] A nonvolatile infrared memory has also been realized in MoS_2/PbS 2D heterostructure FET, where persistent resistance states intrigued by the infrared pulse were exploited.[33] However, so far, except for few reports on new functionalities as data writing and erasing by both electrical and optical routes achieved in MoS_2/PZT FET,[34] exploration of photoelectric FeRAM with 2D/FE heterostructures is seriously deficient.

Herein, we demonstrate a novel nonvolatile photoelectric memory device, constructed in FeFETs consisting of FE thin film PZT and few-layer BP. Charge-mediated electric field control of electronic transport and a unique polarization-dependent photoresponse has been revealed at the PZT-gated BP interface. Furthermore, a nonvolatile memory under the novel "electrical writing-optical reading" processing mode is developed. The device presents excellent stability under long-term FE gating as well as reliable data retention and fatigue performance. We also investigated the coherent synergistic effect through Kelvin probe force microscopy (KPFM) to convince the mechanism of the optical reading of the photoelectric memory. Our approach may pave the way to 2D photoelectric FeRAM and logic circuit with superior performance and malleable fabrication.

Figure 1A shows the 3D schematic of the BP/PZT heterostructure photoelectric memory device on a silicon substrate. The device is in a FeFET structure, with few-layer BP exfoliated on PZT/lanthanum nickel (LNO) layer (thickness: 250/70 nm), which is served as FE gate and made by successive spin coating on Si/SiO_2 (285 nm thick) substrate. In general, 5–10 nm thick BP flakes were chosen as the channel material for the FeFET to guarantee the performance of the device. The purity and crystallinity of the BP were well confirmed by transmission electron microscope (TEM), X-ray photoelectron spectroscopy (XPS), and X-ray diffraction (XRD) characterizations (Figure S1, Supporting Information). The quality of the PZT films was also carefully evaluated before device fabrications, which present very smooth surface (rms roughness: 0.81 ± 0.59 nm) and strong ferroelectricity with negligible leakage under various voltages (Figure S2, Supporting Information). Cr (5 nm)/Au (50 nm) electrodes, which behaves as low Schottky barrier for BP devices, were deposited on top of the BP flakes as contact electrodes. More details about the device fabrication can be referred to Experimental section and Figure S3 (Supporting Information). A typical two-terminal BP/PZT heterostructure FeFET device with channel width/length of 5/8 µm is shown with the optical microscope image (Figure 1B). The inset shows the thickness of the BP flake, which is measured to be ≈6 nm by atomic force microscopy (AFM). Figure 1C presents the cross-sectional topography of the FeFET device, which clearly indicates the thickness of each layer. From the enlarged view of azure dashed ellipse in Figure 1C (Figure 1D), one can find the clean and sharp interface between few-layer BP flake and PZT film, which stacked by van der Waals interaction. Clear layered structure and sharp edges of the BP flake present in Figure 1D also reflects its high crystallinity, where the layer spacing of 0.55 nm (as shown in the insert high resolution TEM(HRTEM) image in Figure 1D) is the signature characteristic of BP.[35] Figure 1E shows the representative Raman spectrum of the BP/PZT heterostructure device on Si substrate, where three characteristic vibrational modes A_g^1, B_{2g}, and A_g^2 of BP were observed besides the 520.9 cm^{-1} peak that for blank PZT/Si substrate. The intensity ratio of the A_g^1 peak of few-layer BP flake here to the Si peak is smaller relative to that of bulk BP, which is consistent with the previous report.[36]

Figure 2A shows a typical hysteresis loop for a PZT capacitor taken at 1 kHz under various voltages. Different voltages (i.e., ±10, ±20, ±30, ±40, ±50 V) were applied to measure the hysteresis loops in order to find a trade-off between high poling voltage to achieve large polarization of PZT films and low gate voltage to tune the conductivity of semiconductor channel. As we can see that a voltage with amplitude of ±10 V is not enough to completely pole the PZT films, but the remnant polarization ≈18.2 µC cm^{-2} at this poling voltage is much higher than that of P(VDF-TrFE) ≈7 µC cm^{-2}, which was used in previously reported FeFET device.[37] The transfer curve of the BP/PZT heterostructure FeFET was measured under a fixed source-drain voltage (V_{ds} = 100 mV) at room temperature (Figure 2B). From the transfer feature, we can see that the proposed device is a typical p-type FeFET. The curve reaches saturation under ±10 V voltage, which indicates that 10 V is enough to make BP channel get fully accumulated or depleted. The mobility μ is plotted and calculated to be a maximum of 202 cm^2 V^{-1} s^{-1} (Figure S4A, Supporting Information). The relatively low mobility of the FeFET device is probably related to the interface states existing in the BP/PZT heterostructures. A hump-like

© 2019 WILEY-VCH Verlag GmbH & Co. KGaA, Weinheim

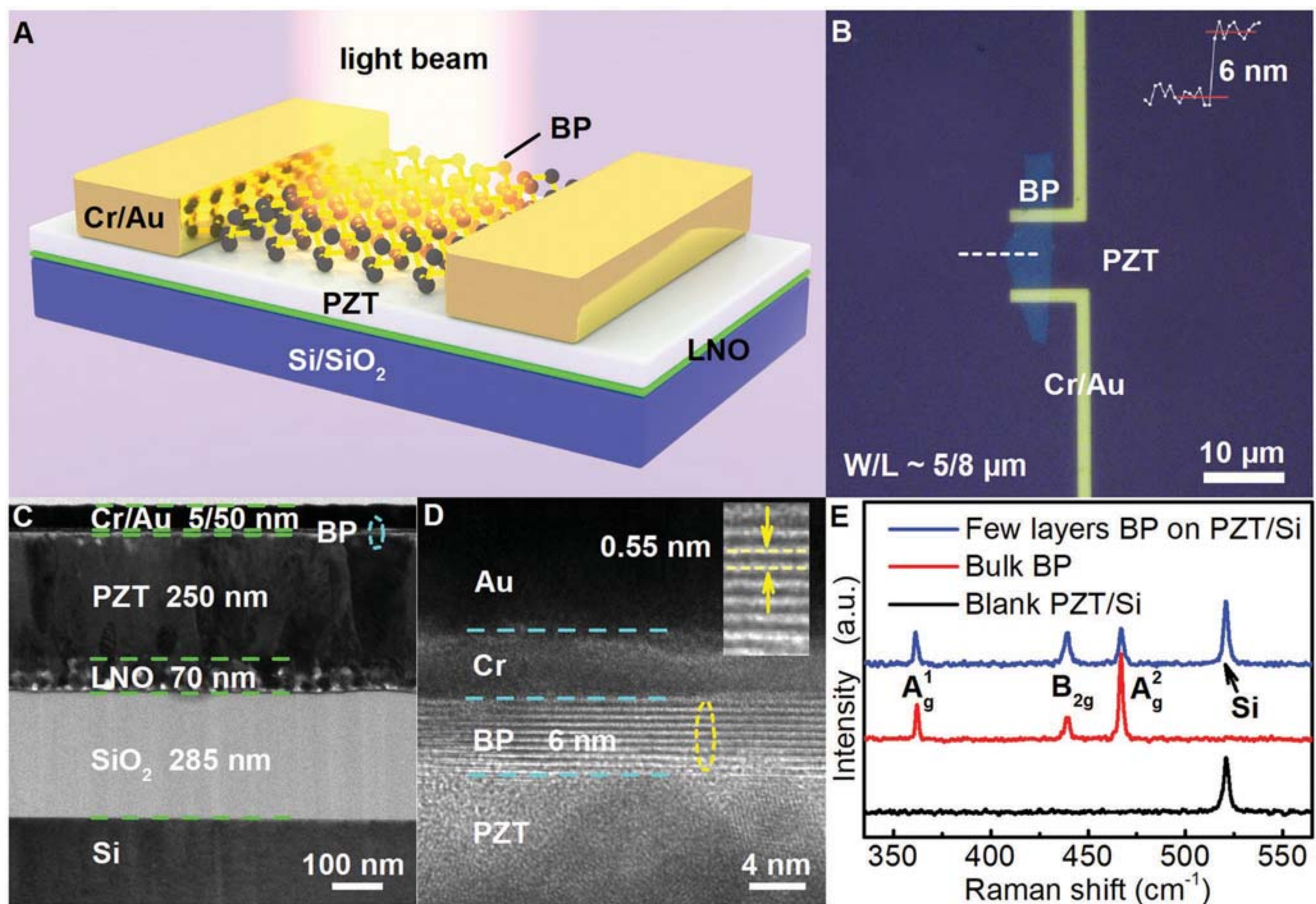

Figure 1. Configuration of the photoelectric memory based on BP/PZT heterostructure BP/PZT FeFET. A) Schematic illustration of the photoelectric memory in FeFET with BP/PZT heterostructure fabricated on $LNO/SiO_2/Si$ substrate. B) Optical image of a typical two-terminal FET device with few-layer BP channel layer and contact electrodes on PZT. Inset shows the AFM line profile of the BP layer with thickness of around 6 nm. Channel width and length of the FET are defined to be 5 and 8 µm, respectively. C) Cross-sectional TEM image of the device. D) HRTEM image of the corresponding BP/PZT heterostructure of the device, marked by a azure dashed ellipse in (C). Inset presents the clear layered structure of the BP with 0.55 nm spacing. E) Raman spectra of few layers BP on PZT/Si, bulk BP, and blank PZT/Si, respectively.

increase of the gate current (I_g) was observed at the gate voltages of $V_g = +4.3$ V and $V_g = -3.7$ V (Figure 2B), which occur near the coercive field of PZT film, indicating the polarization reversal induced fluctuations of the I_g. Output curves at three different ferroelectric polarization states (i.e., fresh state, polarization up state (P_{up}) and polarization down state (P_{down})), were achieved by applying 0, +10, and −10 V respectively with the pulse width of 200 ms (Figure 2C). The output curve at P_{up} is similar to that at fresh state, which indicated the polarization amplitude of these two states are identical to each other and may be caused by self-polarization of PZT film due to sol–gel process–induced residual stress.[38] The piezoelectric force microscope (PFM) phase image (inset of Figure S2C, Supporting Information) also clearly identifies that the fresh state of the PZT film has a self-polarization, which can be seen from the indistinct color contrast between the +10 V switching zone and the nonswitching zone. The BP channel switches to depleted state with abrupt decrease of source-drain current (I_{ds}) when the PZT film turns to P_{down}. The electrical modulation of the FeFET device can be well described through the schematic view of the device at different polarization states together with corresponding equilibrium energy band diagrams (Figure 2D–F). Our result for tuning the conductance of 2D semiconductor channel with ferroelectric polarizations is absolutely different from the previous reports.[14,18,29,37] Here, the interfacial charge effect induced by PZT polarization can better explain the difference of BP channel resistance in different polarization states of PZT.[39,40] A positive pulse voltage, i.e., +10 V applied to the PZT substrate induces negative polarization charges on the top surface of PZT. The negative interfacial charge extracts some of the holes to increase the channel current of 2D BP, meanwhile screening the PZT polarization. On the contrary, positive polarization charges on the top surface of PZT are induced when applied a negative pulse voltage, i.e., −10 V. The positive interfacial charge depletes some of the holes to decrease the channel current of 2D BP. Taking advantage of positive and negative nonvolatile polarization charges, we are able to achieve reversible and nonvolatile modulation of the channel current of 2D BP. Relative to the fresh state (Figure 2D), the holes in the BP channel accumulated arising from negative polarization charges on the top surface of PZT at the P_{up} state (Figure 2E). This may result in the Fermi level (E_F) of BP shifting downward

© 2019 WILEY-VCH Verlag GmbH & Co. KGaA, Weinheim

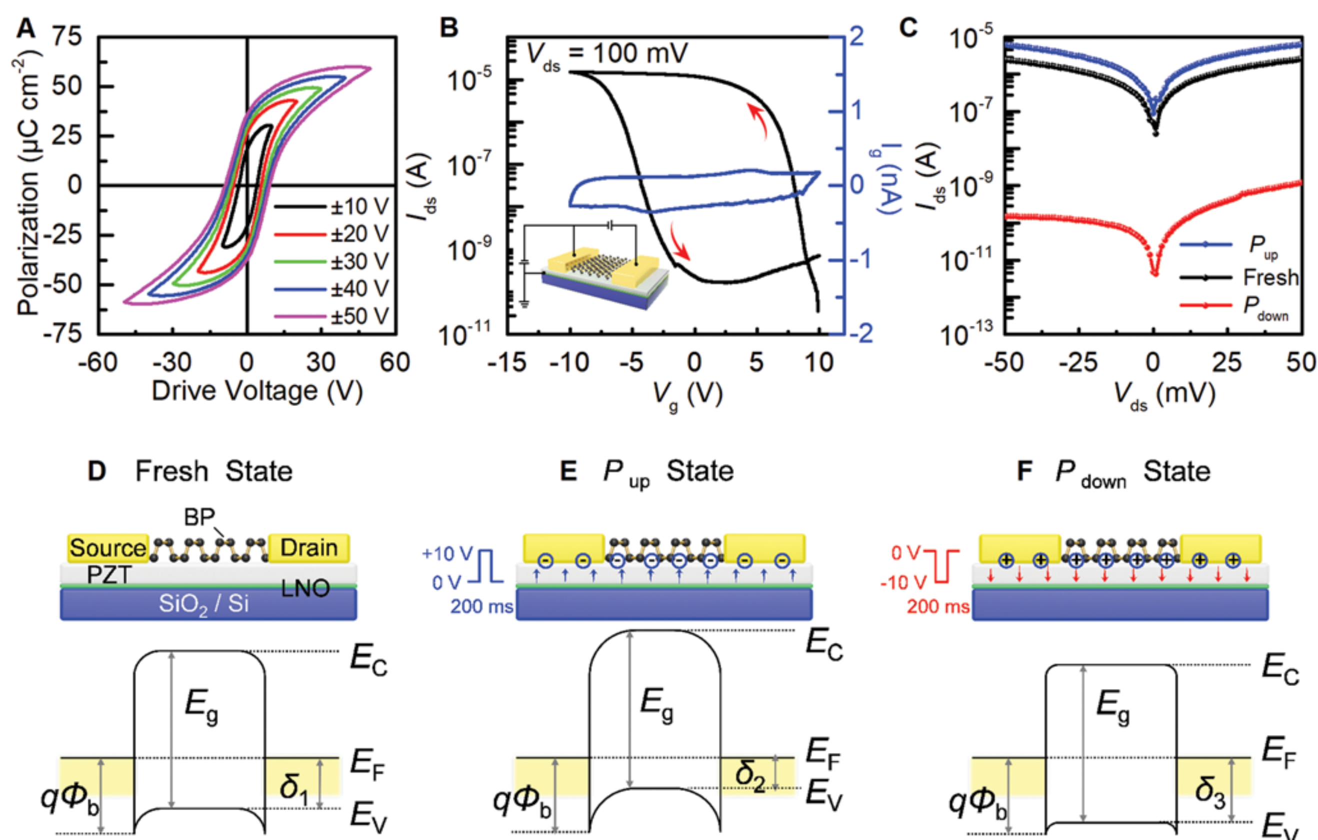

Figure 2. Electrical characteristics of the BP/PZT heterostructure FeFET. A) Typical ferroelectric hysteresis loop of a 250 nm-thick PZT film, measured at different voltage scan scales. B) Transfer curve of a representative ferroelectric gated FET. The leakage current of the device is also presented, with two current peaks occurring near the coercive field of PZT. Inset is the schematic of the BP/PZT heterostructure FeFET with a circuit diagram for the back-gating experiment. C) Output curves of the device obtained in fresh (i.e., pristine ferroelectric PZT film), P_{up} and P_{down} (i.e., P_{up} and P_{down} denote the ferroelectric PZT film was polarized by pulse V_g of 10 V and −10 V, respectively) states. D–F) Schematic illustrations of the device and equilibrium energy band diagrams at V_{ds} = 0 V in fresh D), P_{up} E), and P_{down} F) states, respectively. Hole accumulation and depletion were depicted in the corresponding P_{up} and P_{down} states.

toward valence level (E_V). Meanwhile, the holes accumulation leads to an increased channel current since holes are the majority transport carriers in the p-type FeFET device, which is consistent with the interfacial charge effects. In contrast, when the PZT film is at the P_{down} state, the holes depletion results in decrease of BP channel current (Figure 2F).

The charge-mediated electric field control induced by PZT polarization has significant influence on the photoelectric properties of the FeFET device. Usually, the values of I_{ds} will change as the interfacial charges dissipate over time, so the photoelectrics performance of devices is measured after waiting for almost stability. As shown in **Figure 3**A, the BP/PZT heterostructure FeFET exhibits different photoresponse modes at various polarizations, namely, negative photoconductivity (NPC) for the P_{up} state and positive photoconductivity (PPC) for P_{down} state. We measured the output curves of the BP/PZT heterostructure FeFET at a zero gate voltage after the polarization of the PZT film in the dark and under illumination (808 nm, 30 mW cm^{-2}), respectively. It is found that the photogenerated source-drain current ($I_{laser\ on}$) is smaller than that in the dark ($I_{laser\ off}$) at the P_{up} state, while the $I_{laser\ on}$ is larger than the $I_{laser\ off}$ at the P_{down} state (Figure 3A). To further evaluate the stability and response speed of the FeFET device, the I_{ds} of the device as a function of time were measured by periodically turning on and off the laser light. Figure 3B shows a photoresponse with negligible fluctuations with the periodically illumination at V_{ds} = 10 mV at both P_{up} and P_{down} states, demonstrating the excellent stability and reliability of the device. The response time (t_{on}) is defined as the time for the photocurrent increase from 10% I_{peak} (the maximum value of $I_{laser\ on}$) to 70% I_{peak} and similarly for the recovery time (t_{off}). Then the t_{on} can be determined to be 150 and 230 ms, the t_{off} 300 and 600 ms for P_{up} (Figure 3C) and P_{down} (Figure 3D) states, respectively. The two different response modes are likely attributed to the interface states in the BP/PZT heterostructures, where external electrostatic field may be produced by the charge traps at the PZT domain surface. These interface states may also influence the carrier mobility of the device as we mentioned above in the electrical characteristics analysis. The mechanism for the polarization-dependent photoresponse behavior of the FeFET is expounded and depicted with energy band diagrams shown in Figure 3E,F. The branch point energy E_B (also termed as the charge neutrality level and the Fermi stabilization energy) corresponds to the crossover between predominantly donor-like

 © 2019 WILEY-VCH Verlag GmbH & Co. KGaA, Weinheim

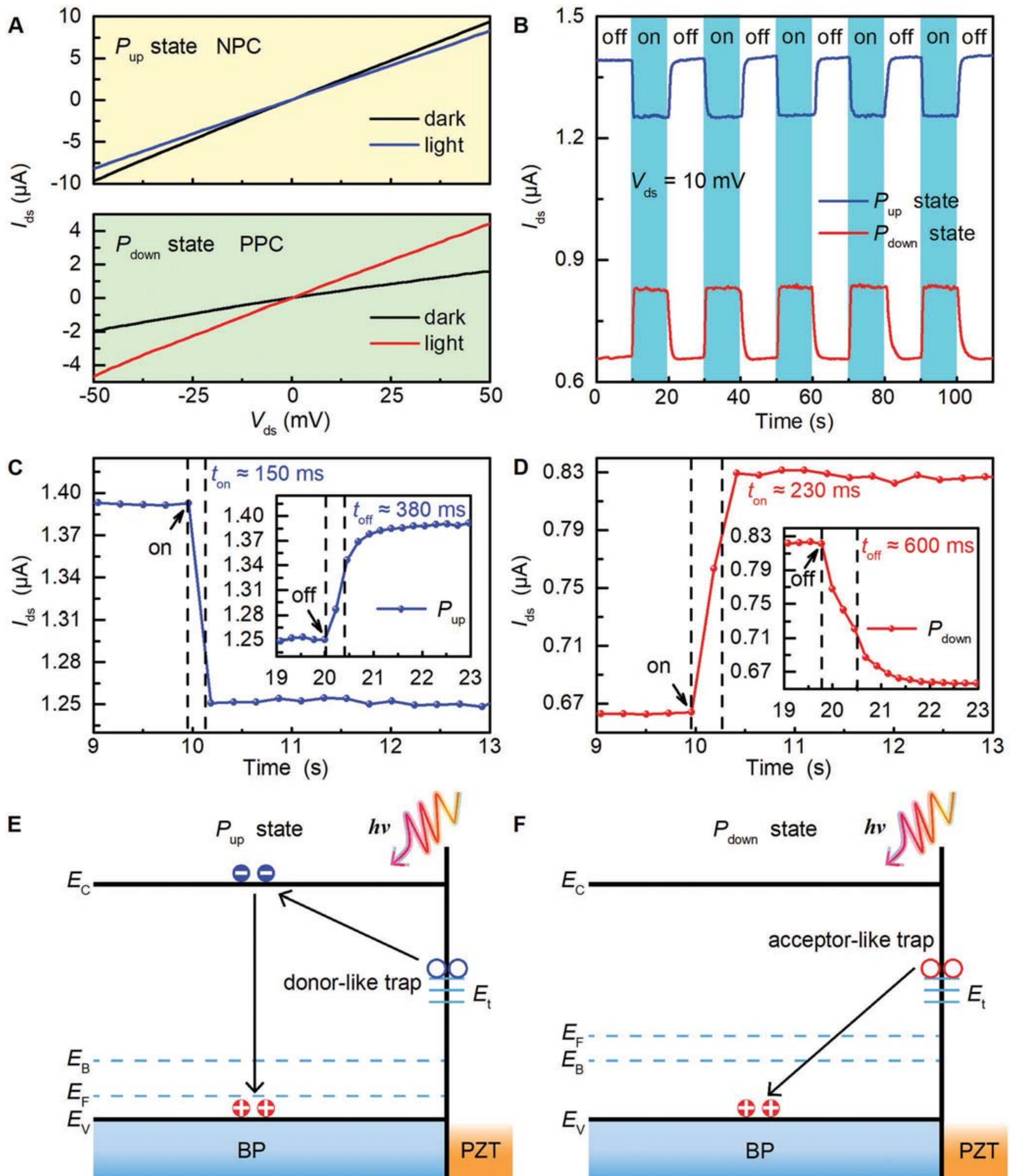

Figure 3. Polarization-dependent photoelectric properties of the BP/PZT heterostructure FeFET. A) Photoresponse of the FeFET in the P_{up} and P_{down} states under identical illumination. PPC and NPC are generated in the same device with ferroelectric gate layer PZT under different polarization states of P_{up} and P_{down}. B) Photoswitching behavior of the FeFET in the P_{up} and P_{down} states at V_{ds} = 10 mV. C,D) The photoresponse time of the BP/PZT heterostructure FeFET device at P_{up} C) and P_{down} D) states. E,F) Schematic illustrations of the mechanism of PPC and NPC within the BP/PZT FeFET when illuminated at P_{up} E) and P_{down} F) states. All the photo-illumination were carried out with a 808 nm laser under P = 30 mW cm^{-2}.

© 2019 WILEY-VCH Verlag GmbH & Co. KGaA, Weinheim

and acceptor-like states.[41,42] To achieve overall charge neutrality, the E_F is always expected to close to E_B. At the P_{up} state, the E_F lies in the vicinity of the E_V with the application of electrostatic field, which lies below E_B. Hence, the interface trap level (E_t) exhibits donor-like state. Under illumination, the electrons from the donor-like traps absorb the photon energy and are excited to the conduction band (E_C). These photogenerated free electrons recombined with the holes from the E_V to cause the observed reduction of holes. Meanwhile, some electrons on the E_V of BP absorb the photon energy and are excited to the E_C, forming electron hole pair and increasing hole concentration. Here, the hole concentration decreases when the recombination is more effective and dominate the photoconductivity, in turn leading to the NPC. While at the P_{down} state, E_F is close to the E_C with the application of electrostatic field, which lies above E_B. Thereby, the E_t exhibits acceptor-like state. When the laser is turned on, the holes from the acceptor-like traps are photoexcited to the E_V and increased the hole concentration. In addition, the photoconductivity process of BP also increased hole concentration, thus resulting in PPC.

On basis of the unique polarization-dependent electrical modulation and photoresponse properties, the BP/PZT heterostructure FeFET has potential applications in nonvolatile photoelectric memory. Under P_{up} and P_{down} states of PZT film with external bias pulse, the BP channel can be either in accumulation or depletion state without further application of V_g, which forms the nonvolatile data information as “1” or “0” of the FeRAM (i.e., electrical writing). A large memory hysteresis window was obtained after long-range V_g dual sweeps from −10 to 10 V at V_{ds} = 100 mV. The V_g pulse height is fixed as −10 V for the “0” state and +10 V for the “1” state while the I_{ds} reaches saturation under ±10 V, manifesting that the charge-mediated electric field control induced by the remnant polarization of PZT is strong enough to cause depletion/accumulation of carriers in the BP semiconducting channel (**Figure 4**A). Afterward, the retention properties of the BP/PZT heterostructure FeFET was measured under low operating voltage V_{ds} = 10 mV and V_g = 0 V after −10 V (“0” state) and 10 V (“1” state) gate voltage pulse for 200 ms respectively, as shown in Figure 4B. The slow degeneration of the I_{ds} is presumably due to charge traps at the interface of BP/PZT heterostructures[34,43] and depolarization field.[14] The I_{ds} of the “0” and “1” states are kept distinctive and almost reach to be stable for over 3600 s. The retention of the nonvolatile photoelectric memory is dependent on the ferroelectric polarization-induced interfacial charge. The advantage of the interfacial charge mechanism is that after removing the applied electric field, two stable residual polarization states of ferroelectric film PZT can be used to realize the nonvolatile regulation of 2D BP, which is beneficial to the storage of nonvolatile information. In principle, it may maintain for a much longer period because these two states mainly depend on the polarization characteristic of the PZT film. Upon illumination, the net generated photocurrent I_{ph} is negative for the P_{up} state and positive for P_{down} (Figure 4C), where the I_{ph} is defined by

$$I_{ph} = I_{\text{laser on}} - I_{\text{laser off}} \quad (1)$$

Consequently, we can obtain the polarization states, which corresponds to the stored information by electrical writing, via detecting the I_{ph}. In particular, the reading process in our BP/PZT heterostructure device is achieved by illumination rather than the electrical route in the traditional FeRAM, resulting in a real nondestructive data reading. More significantly, the proposed reading process can circumvent the challenge of misreading during the electric-reading processes in the traditional FeFET due to their instability issues. Figure 4D shows the dynamic “electrical writing-optical reading” cycles, where the “0” and “1” states were well clarified in the periodic memory cycles (Write “1”-Read- Write “0”-Read). The V_g pulse for the programming and erasing operations were +10 and −10 V for 200 ms, while the illumination for the reading process was with a 808 nm laser pulse in 30 mW cm^{-2} for several seconds, respectively. A stable dynamic response of the I_{ds} current signal was observed. For nonvolatile memory application, the fatigue is also a critical parameter. The fatigue performance of the memory device was evaluated when subjected to the bipolar switching, where no fatigue after more than 500 cycles (Figure S5, Supporting Information). Thus, the function of the FeRAM in a novel operation mode of “electrical writing-optical reading” with nondestructive readout can be readily achieved. Figure 4E schematically shows a 6-cell exemplary photoelectric memory with integrated BP/PZT heterostructure FeFETs array. The FeFET as each cell of the photoelectric memory was assigned the polarization direction (“1” or “0” state) randomly at beginning (I). The data can be electrically written by poling the PZT film in each cell (i.e., electrical writing), as depicted in (II). Then, the data can be optically read by illuminating the whole memory array that the I_{ph} is negative for the “1” state, and positive for the “0” state (i.e., optical reading), as illustrate in (III) and (IV). The concept of the integrated photoelectric memory demonstrated here assumes the feasibility of its scalability.

To further understand the “electrical writing-optical reading” process, the surface potential of the BP/PZT heterostructure FeFET was measured using KPFM during the operations. The data recorded by KPFM is the contact potential difference, which is contrary to the surface potential of sample. The integration of the surface potential change ($\Delta\Psi$) after electrical polarization or light illumination reflects the quantity of electron or hole trapping during processes of the photoelectric memory. Wherefore, KPFM can be an effective tool to confirm the working mechanism of the BP/PZT heterostructure photoelectric memory device. To conduct a reliable comparison, AFM and KPFM images of the fresh BP/PZT heterostructure device were captured in the dark environment, as shown in **Figure 5**A,B, respectively. Figure 5C,E shows the KPFM images on the BP surface for the P_{up} and P_{down} states in dark environment. Relative to the fresh state, the surface potential of the few-layer BP on the PZT film increases (i.e., the image contrast changed from bright to dark) for P_{up} and decreases (i.e., the image contrast changed from dark to bright) for P_{down}. As we know, the accumulation of holes will lead to an increase of the surface potential. Thus, we may obtain that BP channel is in holes accumulation state (“1” state) for P_{up} while holes depletion states (“0” state) for P_{down}. It is in accordance with the electrical modulation of BP/PZT heterostructure FeFET via FE polarization that achieves the electrical writing. Figure 5D,F describes the KPFM images on the BP surface for the P_{up} and P_{down} states upon illumination, respectively. In contrast to those

© 2019 WILEY-VCH Verlag GmbH & Co. KGaA, Weinheim

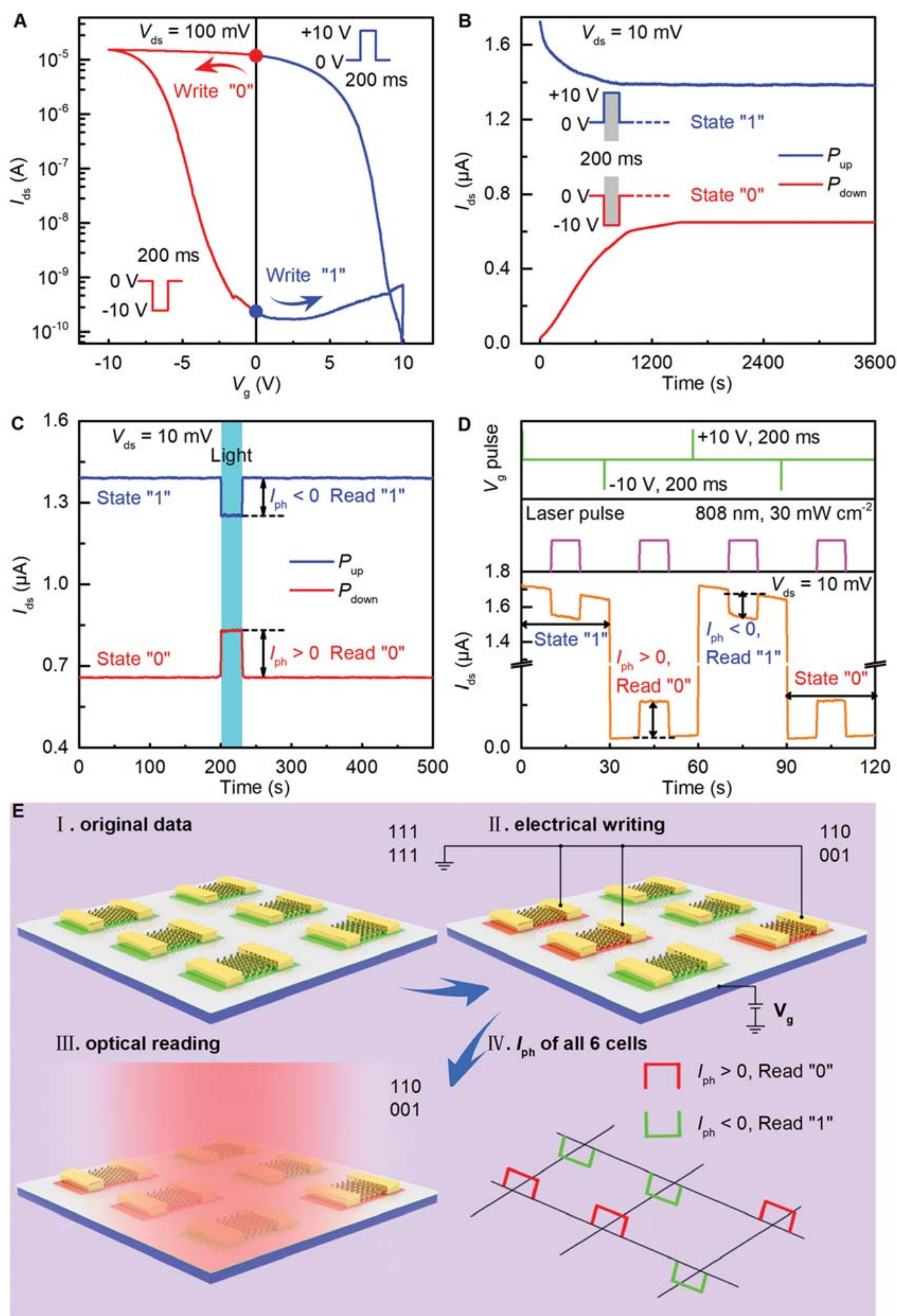

Figure 4. Performance of the photoelectric memory based on BP/PZT heterostructure FeFET. A) Writing with electrical gate pulses. Two obvious memory states of "1" and "0" can be found in the transfer curves (V_{ds} = 100 mV). B) Reading through laser pulses. With the polarization-dependent photoresponse effect, the memory states of "1" and "0" can be read from the changes of the photocurrent with $I_{ph} < 0$ and $I_{ph} > 0$, respectively. C) Retention behavior of the memory. D) Dynamic cycles of the "electrical writing-optical reading" process of the memory. E) Schematic view of a 6-cell photoelectric memory with integrated BP/PZT FeFET array.

 © 2019 WILEY-VCH Verlag GmbH & Co. KGaA, Weinheim

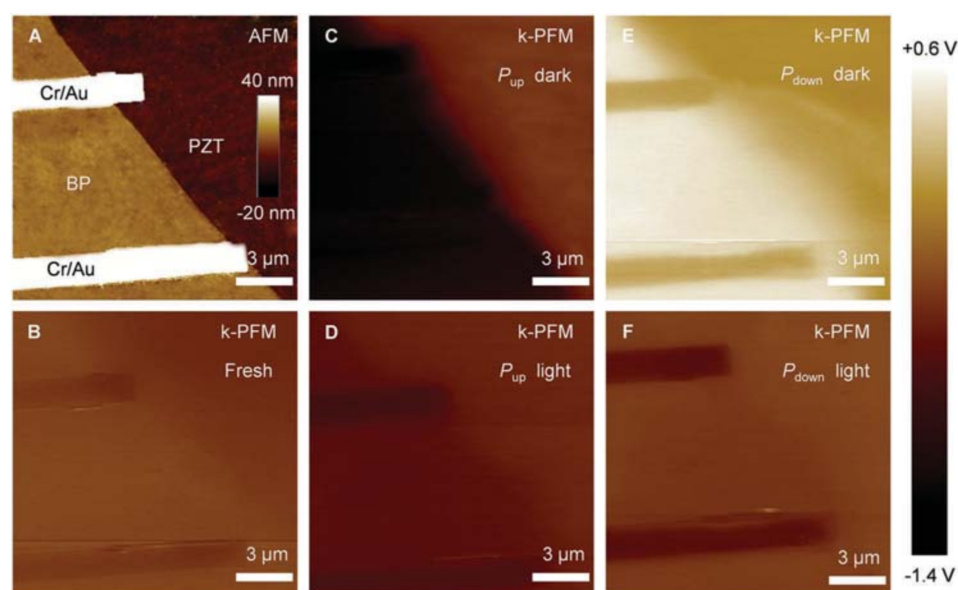

Figure 5. KPFM measurement of the BP/PZT heterostructure FeFET. A,B) AFM A)and KPFM B) images of fresh BP flake on the PZT film surface. C,D) KPFM images obtained after applying a 10 V pulse to the PZT film without C) and with illumination D). Upon illumination, the surface potential of BP decreases for P_{up}, corresponding to NPC. E,F) KPFM images obtained after applying a −10 V pulse to the PZT film without E) and with F) illumination. Upon illumination, the surface potential of BP increases for P_{down}, corresponding to PPC.

measured in the dark, the surface potential of the few-layer BP on the PZT film decreases for P_{up} and increases for P_{down} under light illumination. It is demonstrated that NPC (holes decrease) for P_{up} and PPC (holes increase) for P_{down} is in consistence with the polarization dependent photoresponse. Thereby, the states can be read optically.

In summary, we have demonstrated a nonvolatile photoelectric memory working in a novel "electrical writing-optical reading" mode based on the BP/PZT heterostructure FeFET. With the negative or positive nonvolatile polarization charges induced by polarized PZT thin film, the memory cell persistently holds holes accumulation or depletion without any external voltage bias. Through the synergy effect of BP and PZT, the BP/PZT heterostructure FeFET device exhibits two different photoresponse modes of PPC for the polarization down state and NPC for the polarization up state under illumination, which was confirmed by KPFM. Based on the polarization-dependent photoresponses, the net photocurrent I_{ph} can serve as the readout signal in a memory device. It holds the benefit that the reading can be extremely stable since I_{ph} always own reversed symbols at the "1" and "0" states. This is completely different and superior than the electrical reading of those conventional FeFET memories, where the readout relies on the current on/off ratio that may be degraded while depolarization overtime. Thus, the inherent issue of readout crosstalk within the FeFET memory may be readily resolved. Furthermore, the memory device also exhibits excellent performance for data retention (over 3.6×10^3 s) and fatigue (exceeding 500 cycles). Compared with commercial capacitance FE memory, the "electrical writing-optical reading" type photoelectric memory reported here owns the advantages of stably nondestructive readout, lower energy consumption (driving voltage <10 mV) while benefits in terms of size scaling and COMS compatibility. Our work not only paves the way for the breakthrough of FeRAM devices but also the development of novel functional devices by utilizing the synergy effect between 2D semiconductors and versatile functional materials as ferroelectrics.

Experimental Section

Preparation OF Ferroelectric Functional Thin Film: Before fabrication of FE thin film PZT, LNO thin film was first coated on Si/SiO_2 substrate by sol–gel method and annealed at 700 °C for 10 min. The LNO layer can relieve lattice mismatch between SiO_2 and PZT and can be used as gate electrode. Then PZT thin films were coated on LNO layer by a standard route of sol–gel method.[44] The concentration of the PZT sol was about 0.5 M. And the details of fabrication are mentioned in previous work.[45]

Material Characterizations: The phase and microstructure of the BP and PZT films were characterized using X-ray diffraction (XRD, D8 Advanced, Bruker) with filtered Cu Kα radiation (λ = 1.5406 Å, operating at 45 kV and 200 mA) and field-emission scanning transmission electron microscope (TEM, JEOL JEM-2100F, operating at 200 kV). Raman (LABRAM HR) measurements were performed in a Horiba HR Evolution. The excitation was provided by visible laser light (λ = 532 nm, $P_{in} \approx$ 1.3 μW) through a 100× objective. To analyze elemental composition of the samples, a Thermo Scientific ESCALAB 250Xi X-ray photoelectron spectroscopy (XPS) was used. Thickness was measured with an atomic force microscope (AFM, Dimension ICON). The FE properties of the PZT films were measured by using Radiant Precision Multiferroic. Atomic force microscope and piezoelectric force microscope (AFM/PFM, Bruker Multimode 8) was used to image the surface morphology and ferroelectric domain structures of PZT films. The KPFM images were also measured by AFM, Bruker Multimode 8 system at KPFM module.

Device Fabrication and Measurements: To fabricate the FeFETs, few-layer BP flakes were prepared from bulk BP crystals through the well established mechanical exfoliation method using a blue Nitto tape and transferred on the surface of the PZT layer. The few-layer BP flakes with thicknesses of ≈5–10 nm were usually chosen on the basis of optical contrast and atomic force microscopy (Dimension ICON) measurements. Prior to device fabrication, the substrates with BP thin

© 2019 WILEY-VCH Verlag GmbH & Co. KGaA, Weinheim

flakes were soaked in acetone for several hours to remove the tape residues. The FeFETs were fabricated using electron-beam lithography (JEOL JBX 5500) to define source and drain electrode patterns, electron beam evaporator (ULVAC Ei-5Z) to deposit Cr/Au (5/50 nm) films, and lift-off process to form the source–drain electrodes. Finally the gate electrode LNO was exposed by etching. To avoid oxidation of the BP, the exposure time in ambient during fabrication was controlled within one hour. The electrical characteristics of the FeFETs were measured using a Sussmicrotec probe station and a Keithley 4200 semiconductor parameter analyzer. A solid state laser with infrared light source (808 nm) was used to illuminate the devices. All the measurements were implemented in a vacuum environment (10^{-4} Pa) at room temperature.

Supporting Information

Supporting Information is available from the Wiley Online Library or from the author.

Acknowledgements

L.X. and X.C. contributed equally to this work. This work was supported by the National Natural Science Foundation of China (Grant Nos. 61875223, 51790492, 11574349, and 51572278), the Natural Science Foundation of Jiangsu province (Grant Nos. BK20170424 and BK20160824), the Key Research Program of Frontier Sciences of Chinese Academy of Sciences (QYZDB-SSW-SLH031), the Fundamental Research Funds for the Central Universities (30918012201). The support from the Vacuum Interconnected Nanotech Workstation (Nano-X) of Suzhou Institute of Nano-tech and Nano-bionics (SINANO), Chinese Academy of Sciences is also acknowledged.

Conflict of Interest

The authors declare no conflict of interest.

Keywords

black phosphorus, ferroelectric field effect transistors, heterostructures, nonvolatile photoelectric memory

Received: May 8, 2019
Revised: June 6, 2019
Published online:

[1] T. Parnell, N. Papandreou, T. Mittelholzer, H. Pozidis, *2014 IEEE Global Communications Conference*, IEEE, Piscataway, NJ **2014**, p. 2351.
[2] H. Kim, S. Ahn, Y. G. Shin, K. Lee, E. Jung, *2017 IEEE International Memory Workshop (IMW)*, IEEE, Monterey, California, USA **2017**, p. 1.
[3] Y. Cai, E. F. Haratsch, O. Mutlu, K. Mai, *2013 Design, Automation & Test in Europe Conference & Exhibition*, IEEE, Piscataway, NJ **2013**, p. 1285.
[4] N. Z. Haron, S. Hamdioui, *2008 3rd International Design and Test Workshop*, IEEE, Piscataway, NJ **2008**, p. 98.
[5] C. Liu, X. Yan, X. Song, S. Ding, D. Zhang, P. Zhou, *Nat. Nanotechnol.* **2018**, *13*, 404.
[6] H. Zhang, C. Li, J. Wang, W. Hu, D. W. Zhang, P. Zhou, *Adv. Funct. Mater.* **2018**, *28*, 1805171.
[7] A. Ionescu, H. Riel, *Nature* **2011**, *479*, 329.
[8] H. Shiga, D. Takashima, S. Shiratake, K. Hoya, T. Miyakawa, R. Ogiwara, R. Fukuda, R. Takizawa, K. Hatsuda, F. Matsuoka, Y. Nagadomi, D. Hashimoto, H. Nishimura, T. Hioka, S. Doumae, S. Shimizu, M. Kawano, T. Taguchi, Y. Watanabe, T. Furuyama, *IEEE J. Solid-State Circuits* **2010**, *45*, 142.
[9] H. Ishiwara, *J. Nanosci. Nanotechnol.* **2004**, *12*, 7619.
[10] J. Jiang, Y. Bitla, C.-W. Huang, T. Hien Do, H.-J. Liu, Y.-H. Hsieh, C.-H. Ma, C.-Y. Jang, Y.-H. Lai, P.-W. Chiu, W.-W. Wu, Y.-C. Chen, Y.-C. Zhou, Y.-H. Chu, *Sci. Adv.* **2017**, *3*, e1700121.
[11] M. Dawber, K. Rabe, J. F. Scott, *Rev. Mod. Phys.* **2005**, *77*, 1083.
[12] L. W. Martin, A. M. Rappe, *Nat. Rev. Mater.* **2017**, *2*, 16087.
[13] R. Guo, L. You, Y. Zhou, Z. Lim, X. Zou, L. Chen, R. Ramesh, J. Wang, *Nat. Commun.* **2013**, *4*, 1990.
[14] C. Ko, Y. Lee, Y. Chen, J. Suh, D. Fu, A. Suslu, S. Lee, J. Clarkson, H. Sung Choe, S. Tongay, R. Ramesh, J. Wu, *Adv. Mater.* **2016**, *28*, 2923.
[15] S. Sakai, R. Ilangovan, *IEEE Electron Device Lett.* **2004**, *25*, 369.
[16] S. George, K. Ma, A. Aziz, X. Li, A. Khan, S. Salahuddin, M. Chang, S. Datta, J. Sampson, S. Gupta, V. Narayanan, *2016 53nd ACM/EDAC/IEEE Design Automation Conference (DAC)*, Austin, TX, USA, June **2016**, p. 118.
[17] A. Sharma, K. Roy, *IEEE Electron Device Lett.* **2018**, *39*, 359.
[18] X. Wang, C. Liu, Y. Chen, G. Wu, X. Yan, H. Huang, P. Wang, B. B. Tian, Z. Hong, Y. Wang, S. Sun, H. Shen, T. Lin, W. Hu, M. Tang, P. Zhou, J. Wang, J. Sun, X. Meng, Z. Li, *2D Mater.* **2017**, *4*, 025036.
[19] H. Li, J. Wu, Z. Yin, H. Zhang, *Acc. Chem. Res.* **2014**, *47*, 1067.
[20] X. Chen, C. Chen, A. Levi, L. Houben, B. Deng, S. Yuan, C. Ma, K. Watanabe, T. Taniguchi, D. Naveh, X. Du, F. Xia, *ACS Nano* **2018**, *12*, 5003.
[21] H. Liu, A. T. Neal, Z. Zhu, Z. Luo, X. Xu, D. Tomanek, P. D. Ye, *ACS Nano* **2014**, *8*, 4033.
[22] X. Hong, A. Posadas, K. Zou, C. H. Ahn, J. Zhu, *Phys. Rev. Lett.* **2009**, *102*, 136808.
[23] C. Baeumer, S. Rogers, R. Xu, L. W. Martin, M. Shim, *Nano Lett.* **2013**, *13*, 1693.
[24] S. Yuan, Z. Yang, C. Xie, F. Yan, J. Dai, S. Ping Lau, H. L. W. Chan, J. Hao, *Adv. Mater.* **2016**, *28*, 10048.
[25] T. Li, P. Sharma, A. Lipatov, H. Lee, J.-W. Lee, M. Y. Zhuravlev, T. Paudel, Y. Genenko, C.-B. Eom, E. Tsymbal, A. Sinitskii, A. Gruverman, *Nano Lett.* **2017**, *17*, 922.
[26] C. Yin, X. Wang, Y. Chen, D. Li, T. Lin, S. Sun, H. Shen, P. Du, J. sun, X. Meng, J. Chu, H. F. Wong, C. Wah Leung, Z. Wang, J. Wang, *Nanoscale* **2018**, *10*, 1727.
[27] Y.-J. Doh, G.-C. Yi, *Nanotechnology* **2010**, *21*, 105204.
[28] H. S. Lee, S.-W. Min, M. Park, Y. T. Lee, P. Jin Jeon, J.-H. Kim, S. Ryu, S. Im, *Small* **2012**, *8*, 3111.
[29] Y. T. Lee, H. Kwon, J. Kim, H. Kim, Y. Lee, J. Ah Lim, Y.-W. Song, Y. Yi, W. K. Choi, D. K. Hwang, S. Im, *ACS Nano* **2015**, *9*, 10394.
[30] T. Kobayashi, N. Hori, T. Nakajima, T. Kawae', *Appl. Phys. Lett.* **2016**, *108*, 132903.
[31] Z. Lu, C. Serrao, A. Khan, L. You, J. C. Wong, Y. Ye, H. Zhu, X. Zhang, S. Salahuddin, *Appl. Phys. Lett.* **2017**, *111*, 797.
[32] S. Horiuchi, Y. Tokura, *Nat. Mater.* **2008**, *7*, 357.
[33] Q. Wang, W. Yao, K. Cai, R. Cheng, L. Yin, Y. Zhang, J. Li, Z. Wang, F. Wang, F. Wang, T. A. Shifa, C. Jiang, H. Yang, J. He, *Sci. Adv.* **2018**, *4*, eaap7916.
[34] A. Lipatov, P. Sharma, A. Gruverman, A. Sinitskii, *ACS Nano* **2015**, *9*, 8089.
[35] Y. T. Lee, J. Lee, H. Ju, J. Ah Lim, Y. Yi, W. K. Choi, D. K. Hwang, S. Im, *Adv. Funct. Mater.* **2016**, *26*, 5701.
[36] A. Castellanos-Gomez, L. Vicarelli, E. Prada, J. Island, K. L. Narasimha-Acharya, S. Blanter, D. Groenendijk, M. Buscema, G. Steele, J. Alvarez, H. Zandbergen, J. Palacios, H. S. J. van der Zant, *2D Mater.* **2014**, *1*, 025001.
[37] X. Wang, P. Wang, J. Wang, W. Hu, X. Zhou, N. Guo, H. Huang, S. Sun, H. Shen, T. Lin, M. Tang, L. Liao, A. Jiang, J. Sun, X. Meng, X. Chen, W. Lu, J. Chu, *Adv. Mater.* **2015**, *27*, 6575.

© 2019 WILEY-VCH Verlag GmbH & Co. KGaA, Weinheim

[38] B. Wang, K. W. Kwok, H. L. W. Chan, C. L. Choy, *Appl. Phys. A.* **2004**, *79*, 643.
[39] Q. X. Zhu, M. M. Yang, M. Zheng, R. K. Zheng, L. J. Guo, Y. Wang, J. X. Zhang, X. M. Li, H. S. Luo, X. G. L, *Adv. Funct. Mater.* **2015**, *25*, 1111.
[40] Z.-X. Xu, J.-M. Yan, M. Xu, L. Guo, T.-W. Chen, G.-Y. Gao, S.-N. Dong, M. Zheng, J.-X. Zhang, Y. Wang, X.-G. Li, H.-S. Luo, R.-K. Zheng, *ACS Appl. Mater. Interfaces* **2018**, *10*, 32809.
[41] L. Piper, T. Veal, M. J. Lowe, C. F. McConville, *Phys. Rev. B* **2006**, *73*, 195321.
[42] I. Mahboob, T. Veal, C. F. McConville, H. Lu, W. Schaff, *Phys. Rev. Lett.* **2004**, *92*, 036804.
[43] S. Bertolazzi, D. Krasnozhon, A. Kis, *ACS Nano* **2013**, *7*, 3246.
[44] G. Wang, D. Remiens, E. Dogheche, R. Herdier, X. L. Dong, *J. Am. Ceram. Soc.* **2006**, *89*, 3417.
[45] D. Wang, G. Yuan, G. Hao, Y. Wang, *Nano Energy* **2018**, *43*, 351.

© 2019 WILEY-VCH Verlag GmbH & Co. KGaA, Weinheim